Contour Recognition with a Cooperative Distributed Radar Sensor Network

Andreas Frischen*, Juergen Hasch*, and Christian Waldschmidt†
*Robert Bosch GmbH, Corporate Sector Research and Advance Engineering, P.O. Box 10 60 50, D-70049 Stuttgart, Germany
†Institute of Microwave Techniques, Ulm University, Albert-Einstein-Allee 41, D-89081 Ulm, Germany
Email: {andreas.frischen, juergen.hasch}@de.bosch.com, christian.waldschmidt@uni-ulm.de

***Abstract*—Cooperative Radar Sensor Systems operate several radar sensors with independent generation in a distributed network. Evaluating the cross-echo distances (bistatic responses), additional information about the target's contour can be gained, as the locations of further reflection points of the target can be estimated. In this paper, a system model with several single-channel stations is introduced, which enables to distinguish between spherical (point scatterers) and planar objects. For this model, the complete signal processing chain to process the bistatic response is presented. Criteria to distinguish between point and planar scatterers are derived from geometrical deliberations. The technique is demonstrated in a measurement setup with an arbitrary waveform generator (AWG) as the signal source for two stations. Results are discussed for varying phase noise parameters. The measurements reveal that the presented method enables contour classification of objects under strict phase noise requirements.**

I. Introduction

In recent years, advances in high-speed semiconductor technology, featuring $f_{\max}$ in the range of 300 GHz, lead to the introduction of several highly-integrated radar sensors.[1], [2] These systems integrate several components of a radar sensor on a single chip, including a voltage controlled oscillator (VCO), mixers, amplifiers, couplers and antennas (on-chip or in-package). The main advantage of this single-chip solution over conventional systems with discrete components is that no high-frequency signals (in the 100 GHz range) have to be conducted on the printed circuit board (PCB). Thus, the cost of the PCB can be lowered considerably, due to less strict requirements on material tolerances and the lower complexity of the circuit. On the other hand, the small size strongly limits the possible number of antenna channels. Commonly, only one antenna channel is integrated on the chip or in the package.[1] Recently, a 122-GHz single-chip transceiver with two independent (receiving) antenna channels has been introduced.[2] This enables the estimation of the incident angle at the expense of lower overall antenna performance and therefore lower range.

An approach to extend the capabilities of single-channel sensors is to operate them in a cooperative distributed network. This corresponds to a multiple-input multiple-output (MIMO) radar approach with distributed antennas. Several aspects of this approach have been examined in [3]. Particularly, this approach does not offer a coherent processing gain, but provides a good exploitation of spatial diversity.

In this work, a system structure and signal processing method for a cooperative distributed radar network are introduced. Due to the cooperative aproach, not only the monostatic response of a target at a respective single station but also the bistatic response between the stations and the target can be processed, delivering additional information about the target in terms of the distance to an additional scattering point. It is demonstrated that this information can be used to distinguish between small and extended targets (point and planar scatterers, respectively) by comparison with the expected bistatic distance deduced geometrically. The performance of this technique is evaluated for different phase noise conditions according to the model introduced in [4].

II. System Design

The investigated system constitutes a MIMO radar with widely-separated antennas, where individual signal generation is performed at each antenna position. Therefore, the setup can be regarded as being composed of several independent stations. The aim of the system is to process both the monostatic response (the path from station m to the target to station m) and the bistatic response (the path from station m to the target to station n, with $m \neq n$). Fig. 1 illustrates the overall setup and the signal paths for the signal transmitted at station 1. The paths of the other transmitted signals are omitted for reasons of clarity. Obviously, the processing of the bistatic response delivers additional information about the shape of the target, as further points of reflection are involved.

In order to process the different target responses seperately, the respective response must be extracted from the total received signal, which requires orthogonal impinging signals at the considered station. The separation in the frequency domain is a simple way to achieve this orthogonality. Therefore, the stations operate at (slightly) different fundamental frequencies. In the proposed setup, all stations transmit at the same time, where minor time differences due to imprecise synchronization can be compensated by the signal processing method described in section III-B.

III. Signal Processing

A. Signal Model

An analytical signal model for the cooperative operation of M stations based on the FMCW modulation has been introduced in [4] and is shortly recapitulated and adapted to the system setup of this work in the following.

The FMCW transmit signal of station $m, m \in \{1 \dots M\}$ at position $p_m \in \mathbb{R}^3$ is given by

$$s_m(t) = \exp\left(j2\pi f_m t\right) \exp\left(j\left(\pi k_r t^2 + \phi_{0,m}(t)\right)\right) \quad (1)$$

978-1-4799-7215-9/15/$31.00 ©2015 IEEE

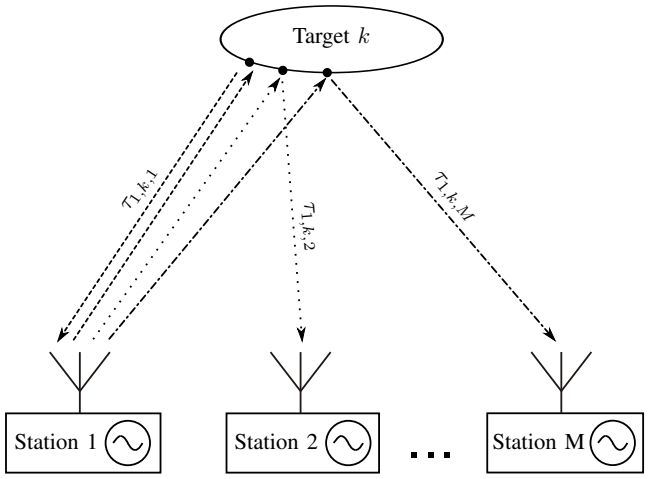

Fig. 1. Paths and reflection points for the signal transmitted at station 1

with the fundamental frequency f_m, phase-noise term $\phi_{0,m}(t)$, and the slope $k_r = \frac{f_{\mathrm{bw}}}{T_{\mathrm{mod}}}$, where f_{bw} represents the bandwidth and T_{mod} the modulation time of the ramp. The phase fluctuation function can be written as

$$\phi_{0,m}(t) = 2\pi f_m \alpha_m(t), \tag{2}$$

where $\alpha_m(t)$ represents a random process with variance $\sigma^2(t) = c_{\mathrm{pn}} \cdot t$. c_{pn} characterizes the strength of the phase noise. Further details on the phase noise model are given in [4] and [5].

The received signal is composed of the sum of all transmitted and reflected signals at all K targets.

$$r_m(t) = \sum_{k=1}^{K} \sum_{n=1}^{M} a_{n,k,m} \cdot s_n\left(t - \tau_{n,k,m}\right) \tag{3}$$

Here, $a_{n,k,m}$ and $\tau_{n,k,m}$ describe the attenuation and travel time from station n to the reflection point on the surface of target k and further to station m, respectively. Subsequently, the received signal is downconverted to baseband by mixing with the transmit signal of station m.

$$r_{m,\mathrm{bb}}(t) = r_m^*(t) s_m(t) \tag{4}$$

In equation 3, the addend with $m = n$ corresponds to the monostatic target response, where the addends with $m \neq n$ correspond to bistatic target responses. While the monostatic response can be processed using traditional techniques, each bistatic response has to be pre-processed as described in the following section.

B. Processing of bistatic response

The calculation of the bistatic distance between the station m, the target k, and the station n requires the baseband signal of both stations m and n. In the following, reciprocity is assumed, i.e. $\tau_{n,k,m} = \tau_{m,k,n}$. Considering only the bistatic target responses from station n to station m, the baseband signal at station m can be written as

$$r_{m,n,\mathrm{bb}}(t) = \sum_{k=1}^{K} a_{n,k,m} \exp\Big(j\big(2\pi(f_m - f_n)t + 2\pi f_n \tau_{n,k,m} + 2\pi k_r \tau_{n,k,m} t - \pi k_r \tau_{n,k,m}^2 + \phi_{0,k,n}(t)\big)\Big) \tag{5}$$

Thus, the baseband signal is composed of several FMCW target responses shifted in the frequency domain by $f_m - f_n$. For $f_m < f_n$, the analytical frequency becomes negative while the observed real frequency is positive with the frequency peaks of the target responses reverted in the frequency domain, i.e. larger distances lead to lower frequencies. The effective phase noise term $\phi_{0,m,n}(t) = \phi_{0,m}(t) - \phi_{0,n}(t - \tau_{n,k,m})$ has been analyzed in [4].

The processing comprises the following steps:

1) Convert both baseband signals to frequency domain
2) Extract the respective portion around $f_{\mathrm{off}} = |f_m - f_n|$
3) Convolve the two extracts
4) Determine the exact $f'_{\mathrm{off}} = f_{\mathrm{off}} + \triangle f$ by finding the peak frequency in the convolved spectrum
5) Shift both frequency domain signals by f'_{off} and revert the inverted spectrum
6) Further process as quasi-homodyne response

Step 1 yields the two spectra with frequency peaks at $f'_{\mathrm{off}} \pm k_r \tau_{n,k,m} = f_{\mathrm{off}} + \triangle f \pm k_r \tau_{n,k,m}$, where $\triangle f$ corresponds to the additional frequency offset due to imprecise synchronization and the $\pm$ refers to the reverted spectrum at one of the stations. For step 2, an adequately large frequency range has to be selected, so that it assuredly extends over f'_{off}. The convolution of the two spectra (step 3) is equivalent with the correlation with the reverted spectrum. Thus, the convolution reaches its maximum at $2f'_{\mathrm{off}}$, where the superimposed spectra are congruent, delivering the wanted f'_{off} of step 4. In the next step, the spectra can be shifted by this value to the homodyne region, while one extract has to be reverted, additionally. Finally, the resulting spectra can be further processed in the same way as the monostatic target responses. As both spectra carry the same information, only one of them has to be processed to find the travel times $\tau_{n,k,m}$ and distances $d_{n,k,m} = c_0 \cdot d_{n,k,m}$, where c_0 represents the speed of light.

Note that the convolution in the frequency domain (step 3) can be replaced by the less computationally complex multiplication in the time domain. In this case, the convolution is effectively performed cyclically, due to the Fourier transform properties of finite-length signals. Therefore, a higher oversampling rate is necessary for the sampling of the time-domain signal to retain unambiguity. If the signals are multiplied in the time-domain, the approach is similar to the one presented in [6], with the difference that in the latter a coherent processing with closely arranged stations was attempted.

As with a single sensor no angular information can be acquired, the monostatically determined distances $d_{m,k,m}$ yield a circle as the set of points for the estimated scatterer position. Analogously, the bistatically determined distances $d_{n,k,m}, m \neq n$ each yield an ellipse as the set of points for the estimated scatterer position. The parameters a and b of this ellipse are given by (6) and (7), respectively.

$$a_{\mathrm{ellipse}} = \frac{d_{n,k,m}}{2} \tag{6}$$

$$b_{\mathrm{ellipse}} = \sqrt{\left(\frac{d_{n,k,m}}{2}\right)^2 - \left(\frac{|p_m - p_n|}{2}\right)^2} \tag{7}$$

In the case of a point scatterer, the circles and ellipses intersect in a single point. In the case of planar objects, the main

978-1-4799-7215-9/15/$31.00 ©2015 IEEE

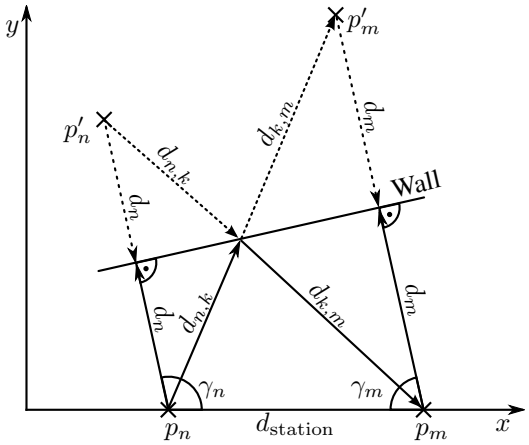

Fig. 2. Bistatic distance $d_{n,k,m}$ for a planar object (wall)

scatterers are different points on the surface of the object, so that no single point of intersection is observed.

C. Criterion for classification

The common point of intersection in the case of a point scatterer leads to the bistatic distance

$$d^{\text{point}}_{n,k,m} = \frac{d_{n,k,n} + d_{m,k,m}}{2}. \tag{8}$$

The case of a planar scatterer is depicted in Fig. 2. Here, the law of cosines is applied for the two large triangles extending to the stations' mirrored positions.

$$d^2_{n,k,m} = d^2_{\text{station}} + (2d_m)^2 - 2d_m \cos(\gamma_m) \tag{9}$$

$$d^2_{n,k,m} = d^2_{\text{station}} + (2d_n)^2 - 2d_n \cos(\gamma_n) \tag{10}$$

Using the equivalents $d_{n,k,m} = d_{n,k} + d_{k,m}$, $d_{m,k,m} = 2d_m$, and $\gamma_m + \gamma_n = 180$ together with (9) and (10) leads to the bistatic distance for a planar scatterer

$$d^{\text{planar}}_{n,k,m} = \sqrt{d^2_{\text{station}} + d_{n,k,n} \cdot d_{m,k,m}}. \tag{11}$$

The comparison of the observed bistatic distance with the respective expected distance according to 8 and 11 allows the classification of the target as a point or planar scatterer.

IV. Results

Measurements have been taken with a setup of 2 stations and 2 different targets: an aluminum-coated partition screen and a metallic sphere with $d = 24\,\text{cm}$. These two objects represented a planar and a point scatterer, repectively. The transmit signals for the stations have been generated by an arbitrary waveform generator (AWG), which enabled the incorporation of arbitrarily strong phase noise. The signal of each station was fed to a horn antenna through a coupler. The antennas were positioned at $p_1 = (-0.25, 0, 0)^{\text{T}}$ and $p_2 = (0.25, 0, 0)^{\text{T}}$, respectively, according to Fig. 2. The targets were positioned at a distance of approx. 2.8 m. In the receiving direction, the signal was fed to a mixer, together with the respective transmit signal for downconversion. The RF setup is illustrated in Fig. 3. The used parameters are summarized in Table I. The phase noise parameter c_{pn} has been

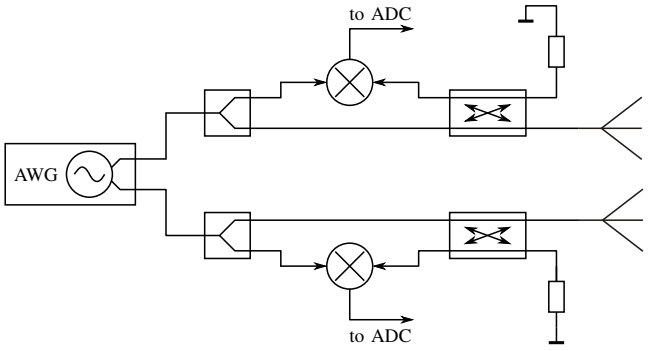

Fig. 3. Measurement setup with AWG signal generation

TABLE I. Measurement Parameters

Fundamental frequency	f_0	5.8 GHz
Frequency offset	$f_m - f_n$	500 kHz
Modulation bandwidth	f_{bw}	500 MHz
Modulation time	T_{mod}	1 ms
AWG sampling frequency	$f_{\text{sample,AWG}}$	25 GS/s
IF sampling frequency	$f_{\text{sample,IF}}$	2 MS/s
Distance between stations	d_{station}	0.5 m

varied from $c_{\text{pn,min}} = 10^{-21}\,\text{s}^2\text{Hz}$ to $c_{\text{pn,max}} = 10^{-15}\,\text{s}^2\text{Hz}$ in one to two steps per decade. Note that the frequency offset $f_m - f_n$ was fixed with almost perfect synchronization, but to test the performance of the algorithm, this information was not used within the evaluation.

The discussed circles and ellipses representing possible reflection positions are depicted in Fig. 4 and 5 for a small spherical and planar scatterer, respectively. As expected, all curves intersect in a single point in the case of a small spherical (point) scatterer, while different reflection points on the wall lead to no common point of intersection.

The robustness of the algorithm in section III-B to find the correct f'_{off} has been examined for different phase noise conditions and plotted in Fig. 6 for the spherical target. Up to a phase noise value of $c_{\text{pn}} = 10^{-18}\,\text{s}^2\text{Hz}$, equivalent to a single-sideband power spectral density of $\mathcal{L}(100\,\text{kHz}) = -85\,\frac{\text{dBc}}{\text{Hz}}$, the algorithm estimates the offset frequency f'_{off} precisely.

In order to complete the presented method of distinguishing between point and planar scatterers, the observed bistatic distances are compared to the expected values for both cases. For each target, the bistatic distances for a point and

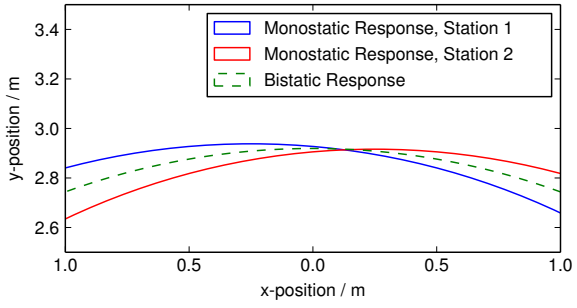

Fig. 4. Detected reflection distances for a small spherical scatterer

978-1-4799-7215-9/15/$31.00 ©2015 IEEE

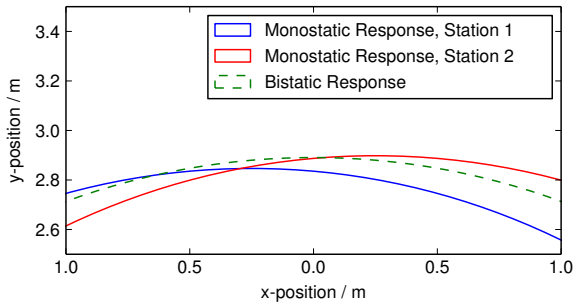

Fig. 5. Detected reflection distances for a planar scatterer (wall)

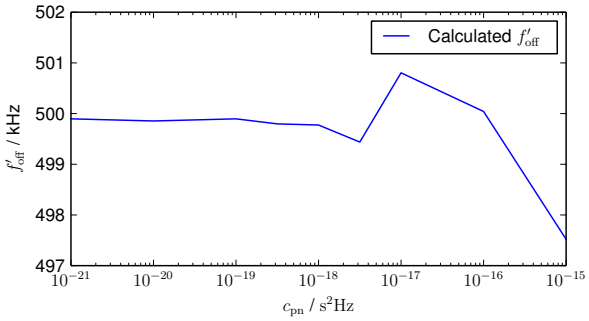

Fig. 6. Calculated f'_{off} for different phase noise parameters c_{pn}

planar scatterer are calculated from the monostatic distances according to (8) and (11), respectively. The observed bistatic distances are plotted together with these values in Fig. 7 and 8 against different phase noise values c_{pn}. As the monostatic measurements have a minor dependence on the phase noise, the bistatic distances calculated from them, are almost constant. It becomes apparent, that the precision of the estimated distance is not sufficient for $c_{\text{pn}} = 10^{-18}\,\text{s}^2\text{Hz}$, despite the correctly estimated f'_{off}. For lower phase noise, the small spherical target can be reliably identified as point scatterer, while for the wall a distinctly larger bistatic distance is observed. Apparently, there are reflections from other scatterers such as edges and the metallic frame of the partition screen involved, that superimpose the reflections from the aluminum coating. Therfore, the observed bistatic distance does not completely reach its expected value of an ideal planar object.

V. Conclusion

In this work, a method to recognize the contour of an object using a cooperative distributed radar sensor network and processing the bistatic response between the stations has been introduced. A robust signal processing technique to estimate the bistatic distance has been presented. The relation of the bistatic and monostatic distances of point and planar scatterers have been derived from geometric calculations, enabling the distinction by comparison with the observed distances. In a measurement setup, the effectiveness of the proposed system design and signal processing has been proven. Examinations under varying phase noise conditions reveal, that the application of the presented method with the used modulations parameters requires a maximum phase noise equivalent to a single-sideband power spectral density of $\mathcal{L}(100\,\text{kHz}) = -90\,\frac{\text{dBc}}{\text{Hz}}$ for the signal sources.

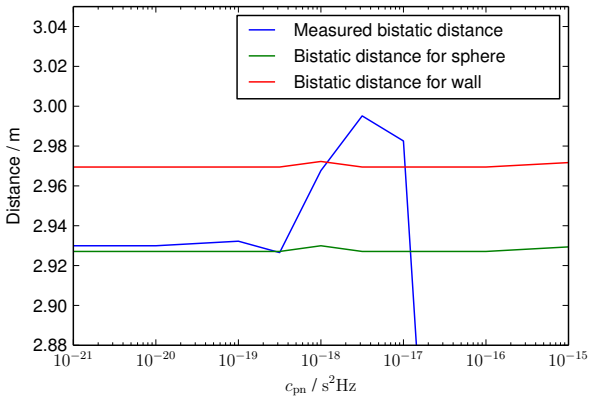

Fig. 7. Measured bistatic distance for scene with point scatterer compared to expected distances for both targets

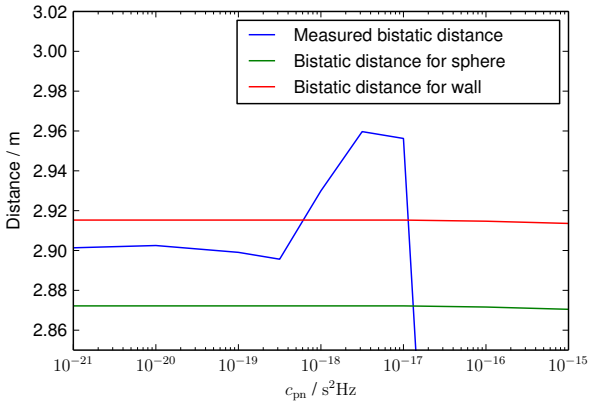

Fig. 8. Measured bistatic distance for scene with planar scatterer compared to expected distances for both targets

References

[1] M. Girma, S. Beer, J. Hasch, M. Gonser, W. Debski, W. Winkler, Y. Sun, and T. Zwick, "Miniaturized 122 GHz system-in-package (SiP) short range radar sensor," in *10th European Radar Conference (EuRAD)*, Oct 2013, pp. 49–52.

[2] M. G. Girma, J. Hasch, M. Gonser, Y. Sun, and T. Zwick, "122 GHz single-chip dual-channel SMD radar sensor with integrated antennas for distance and angle measurements," in *44th European Microwave Conference (EuMC)*, Oct 2014, pp. 1754–1757.

[3] A. Haimovich, R. Blum, and L. Cimini, "MIMO radar with widely separated antennas," *IEEE Signal Processing Magazine*, vol. 25, no. 1, pp. 116–129, 2008.

[4] A. Frischen, J. Hasch, and C. Waldschmidt, "Performance degradation in cooperative radar sensor systems due to uncorrelated phase noise," in *11th European Radar Conference (EuRAD)*, Oct 2014, pp. 241–244.

[5] A. Demir, A. Mehrotra, and J. Roychowdhury, "Phase noise in oscillators: a unifying theory and numerical methods for characterization," *IEEE Trans. Circuits Syst. I, Fundam. Theory Appl.*, vol. 47, no. 5, pp. 655–674, May 2000.

[6] R. Feger, C. Pfeffer, C. Schmid, M. J. Lang, Z. Tong, and A. Stelzer, "A 77-GHz FMCW MIMO radar based on loosely coupled stations," in *The 7th German Microwave Conference (GeMiC)*, March 2012, pp. 1–4.

978-1-4799-7215-9/15/$31.00 ©2015 IEEE